Journal of
Nanomedicine & Nanotechnology

Zou et al., J Nanomed Nanotechnol 2015, 6:6
DOI: 10.4172/2157-7439.1000339

Research Article Open Access

Size Effects of Nanocomplex on Tumor Associated Macrophages Targeted Delivery for Glioma

Lei Zou, Alejandro Macias sustaita, Tima Thomas, Lihn Do, Juan Rodriguez and Huanyu Dou*

Department of Biomedical Sciences, Texas Tech University Health Sciences Center, Paul L. Foster School of Medicine, El Paso, Texas, USA

Abstract

The size of functional nanocomplexes, which targets the brain tumor associated macrophages nanocomplex plays a very important role in their interaction with cells involving uptake, release and targeting selectivity. The size effects of nanocomplex on cell-based targeted delivery were studied to investigate if this phenomenon can be employed to combine the targeting peptide to provide a selective tumor associated macrophages targeted delivery system for anti-glioma therapy. Paclitaxel (PTX) was loaded into a core-shell structure of nanocomplex (PTX-Nanocomplex). Three different sizes of PTX-nanocomplex were prepared through nanoprecipitation. Rabies virus glycoprotein (RVG) peptide was conjugated to PTX-nanocomplex to form RVG-PTX-nanocomplex. Uptake, release, transportation and anti-glioma activities were studied in *in vitro* by using bone marrow derived macrophages (BMM) and tumor associated macrophages (TAMs), human glioma U87 cells, and neurons. The resulting RVG-PTX-nanocomplex had a spherical shape, with the size of 72 nm (small), 138 nm (medium), and 220 nm (large). The large-size RVG-PTX-nanocomplex showed greater uptake by BMM, but did not take by neurons. Co-cultivation of U87 and TAMs pre-loaded with large-size RVG-PTX-nanocomplexes provided significant anti-glioma activities. More importantly, large-size RVG-PTX-nanocomplexes were selectively targeted to TAMs and effectively transported to U87 cells with lower side effects. We concluded that the large-size RVG-PTX-nanocomplex had promising potential uses in the TAMs targeted delivery system for glioma therapy.

Keywords: Size effect; Nanocomplex; Rabies virus glycoprotein (RVG); Anti-glioma

Introduction

Glioma is the most lethal primary brain tumor [1,2]. The survival rates of patients with malignant gliomas have not improved significantly in past 4 decades, with less than one year survival rate after diagnosis [1-4]. Surgery, radiation and chemotherapy are the most common treatment of malignant glioma. However, because of its invasive nature, glioma mass is particularly difficult to be separated from the normal tissue and removed from disease site. Therefore, the poor penetration of the therapeutic agents across the BBB makes the currently available medicines ineffective.

PTX is very effective against a wide variety of solid tumor cancers [5]. However, it has very poor aqueous solubility leading to low therapeutic index, and side effects including nausea, vomiting, loss of appetite, change in taste, thinned or brittle hair, and pain in the joints. Numerous studies have aimed to develop the nano-PTX delivery systems, including polymeric micelles [6], liposomes [7,8], microspheres [9], nanoparticles [6,10-13], PTX-polymer conjugates [14-16] and dendritic polymers [15]. Targeted delivery PTX-nanoparticels are deemed as the most promising approaches [17-21]. When nanotechnology is applied to drug delivery systems, targeted delivery of anti-cancer nano-drug offer greater tumor selectivity and improved pharmacokinetics [17-21].

A delivery constraint to treat glioma arises due to the restrictive permeability of the brain capillary endothelium that forms the BBB [22,23]. It is important to consider not only the delivery of drugs to the CNS, but also their ability to access the relevant target site within the brain. RVG peptide [22], a short peptide derived from rabies virus glycoprotein, has been used as a brain targeting ligand to deliver bioactive agents into the brain [23-28]. By binding to the AChR in the vascular endothelium of the BBB, RVG plays an important role in allowing transvascular delivery specifically to cross the BBB and to target the brain [24,29-35].

One of the pathological features of glioma is that tumor associated macrophages/microglia (TAMs) express high levels of AChR and support tumor growth [36,37]. Remarkably, the abundance of those TAMs correlates with the grade of malignancy [36,38-42], which could provide a relatively specific means for glioma-specific targeted delivery [43,44]. In addition, activation of microglia/macrophages has a greater ability to phagocytose and take up nano-drug followed by exocytosis of the particles in order to release the drug within tumor tissue.

There are countless studies on the synthesis, encapsulation, surface modification, and toxicity of nanoformulations [45-47]. On the other hand, it is obvious that the size parameter of nanostructures plays a very important role when they interact with live cells. The size effect of nanoformulation on targeting specificity and pharmacokinetical activities remains very poorly understood. There are very few investigations of particle size effect on the uptake and intracellular behavior, which will promote the practical applications of nanotechnology based drug delivery systems [48-50]. Very recently, we developed a RVG peptide conjugated PTX-nanocomplex (RVG-PTX-nanocomplex). RVG-PTX-nanocomplex, with a mixed lipid monolayer shell, a biodegradable polymer core, and targeting RVG peptide, had good uptake, controlled release, effective anti-glioma activities and preferentially across the BBB to target TAMs. In this

***Corresponding author:** Huanyu Dou, MD, Department of Biomedical Sciences, Texas Tech University Healthe Sciences Center at El Paso, El Paso, TX 79905-2827, Tel: 915-215-4259; Fax: 915-783-1253; E-mail: huanyu.dou@ttuhsc.edu

Received September 03, 2015; **Accepted** November 16, 2015; **Published** November 26, 2015

Citation: Zou L, Sustaita AM, Thomas T, Do L, Rodriguez J, et al. (2015) Size Effects of Nanocomplex on Tumor Associated Macrophages Targeted Delivery for Glioma. J Nanomed Nanotechnol 6: 339. doi:10.4172/2157-7439.1000339

study, we further formulated and selected varied sizes of RVG-PTX-nanocomplex to study the in vitro behavior to optimize this delivery system. By adjusting the PLGA polymer concentration in the process of nanoprecipitation, which we chose for the preparation of the nanoparticles, we successfully obtained RVG-PTX-nanocomplexes with three sizes at ~ 72 nm, ~ 138 nm, and ~ 220 nm, respectively. We found that the larger size of RVG-PTX-nanocomplex had a slower release of the drug, and at the same time, the different sizes did not affect toxicity to the tumor cells. Importantly, the larger size of RVG-PTX-nanocomplex was specifically taken by macrophages, but not taken by neurons. The size-controlled RVG-PTX-nanocomplex, of the size ~ 220 nm, are more suitable for a macrophage based drug delivery system for brain TAMs targeted delivery to treat glioma [51-54].

Materials and Methods

Materials

Poly (D,L-lactide-co-glycolide) (50/50) with terminal carboxylate groups (PLGA; inherent viscosity, 0.55 - 0.75 dl/g in hexafluoroisopropanol; MW: ~ 44 kDa) was obtained from Absorbable Polymers International (Pelham, AL, USA). The hydrogenatedL-α-phosphatidylcholine (Soy) (HSPC, MW: 762) and DSPE-PEG-Mal (1,2-distearoyl-sn-glycero-3-phosphoethanolamine-N-[Maleimide(polyethylene glycol)-2000]) were obtained from Avanti (Alabaster, AL). The peptide RVG with cysteine at the C-terminus (YTIWMPENPRPGTPCDIFTNSRGKRASNGGGGC, HS-RVG) was synthesized by RS Synthesis (USA) Ltd. β-Mercaptoethano (βME) and tetramethylrhodamine-5-maleimide (TRM) was obtained from Sigma - Aldrich. Lissaminerhodamine B 1,2-dihexadecanoyl-sn-glycero-3-phosphoethanolamine, Rhodamine 6G (Sigma-Aldrich) was used as red fluorescence label.

Preparation of PTX-nanocomplex

Lipid-PLGA-PTX-nanocomplex was synthesized using a modified nanoprecipitation technique combined with self-assembly, as described previously [55-59]. Briefly, for the preparation of small nanoparticle, PLGA, PTX (10% of the weight of PLGA) and Rhodamine 6G (2% of the weight of PLGA) were first dissolved in N,N-Dimethylmethanamide (DMF) at PLGA concentration of 3 mg/mL. HSPC and DSPE-PEG-Mal (8/1, molar ratio) were dissolved in a 4% ethanol aqueous solution at 120% PLGA polymer weight and heated to 65°C. The PLGA/acetonitrile solution was then added drop-wise into the preheated lipid aqueous solution (1 mL/min) under gentle stirring. The nanocomplex was allowed to self-assemble for 2 h with continuous stirring while the organic solvent was allowed to evaporate. The remaining organic solvent and free molecules were removed by washing the NP solution three times using an Amicon Ultra-4 centrifugal filter (Millipore, Billerica, MA) with a molecular weight cut-off of 100 kDa, and nanocomplex stock solution with the concentration of about 15 mg/mL was obtained. The nanocomplex was used within one week and stored at 4°C.

Preparation of RVG-PTX-nanocomplex

Commercial HS-RVG (1 mg/mL) was reduced by βME (5 eq.) in aqueous solution. After 4 h, PTX-nanocomplex (10 eq.) stock suspension (10 mg/mL) was added and reacted for 24 h at room temperature in dark. The Maleimide groups of the PTX-nanocomplex specifically reacted with the thiol groups of HS-RVG. The resulting RVG-PTX-nanocomplexes were washed with ultrapure water (15 mL) by ultrafiltration, concentrated, and the stock suspension was kept at 4°C until use.

RVG-PTX-nanocomplex characterization

The average particle size and size distribution of the nanocomplex were measured using a Malvern Zetasizer Nano ZS Dynamic Light Scattering (DLS) instrument. The shape and surface morphology of the nanocomplex were investigated by atomic force microscopy (AFM), and 100 mL of PTX-loaded NP solution was placed on a clean mica surface and then air-dried overnight. Images were obtained with a Park AFM system. The drug encapsulation efficiency (EE%) was calculated as: (actual amount of drug encapsulated)/(initial amount of drug used in the fabrication) × 100%. The drug loading fraction (DL%) were calculated as: weight of PTX in nanocomplex/weight of the nanocomplex × 100%.

PTX release from nanocomplex

The suspensions of RVG-PTX-nanocomplex containing the same amount of paclitaxel were placed into a 1 mL dialysis membrane tubing (MWCO 3500, Spectrum Laboratories, Inc.) and dialyzed against 100 mL PBS with 0.1% Tween 80. At each fixed time points, samples of 2 mL of the release media was collected and compensated with an equal volume of the fresh release media. The samples were freeze-dried, thoroughly extracted with acetonitrile, and the released amounts of PTX were determined by HPLC.

The PTX concentration of the solution was determined by reversed phase HPLC (RP-HPLC) using a Phenomenex Luna C18 column isocratically eluted with a 60:40 v/v acetonitrile/water. The system was run at a flow rate of 0.8 mL/min, and PTX was detected at 227 nm. The concentration of PTX in the solution was determined by the peak area using a standard curve obtained with fixed concentrations of PTX in acetonitrile.

BMM, TAMs and U87 cells cultures

Using a protocol approved by the Institutional Animal Care and Use Committee (IACUC), mouse (Balb/C, male 4-6 weeks) femur bone marrow was dissociated into single-cell suspensions. Bone marrow cells were cultured in DMEM with fetal bovine serum (10%), penicillin, streptomycin, and 500 U/ml. Macrophage-colony stimulating factor (MCSF) is not only an important regulator of macrophage production, but also stimulates macrophages/monocyte polarization into TAMs under pathological condition. TAMs are believed to represent proliferation of macrophage progenitor cells within the tumor microenvironment. BMMs were supplied with MCSF and co-stimulation by glioma U87 cultured medium to differentiate into TAMs. Human glioma U87 cells labeled with green fluorescence (GFP-U87) and embryonic mouse hippocampal cell lines (neuron cells, mHippoE-14) were cultured in DMEM supplemented with 10% fetal bovine serum.

MTT assay

For the MTT assay, cells were plated on 96-well plates and treated to RVG-PTX-nanocomplexes and PTX-nanocomplexes containing same amount of PTX, and free PTX. The cells were incubated to experimental time. Then, to each well the medium was replaced by 100 μL of MTT solution (5 mg/mL solution in 10% fetal bovine serum (FBS) in phosphate buffered saline (PBS)) was added and incubated for 45 min at 37°C. At the end of the incubation period, with 100 μL of dimethyl sulfoxide (DMSO) was replaced and the plate was moderately shaken for 15 min at room temperature to let the purple formazan crystals dissolve. Absorbance at 490 nm was measured with an ELISA microreader.

Flow cytometry

The cells were collected and fixed with 4% paraformaldehyde. Data were acquired by BD FACS Canto II and analyzed on BD FACS Diva software. PE channel was used for the detection of fluorescence.

Uptake by BMM and neuron

BMM and neurons were incubated with medium containing three different sizes of RVG-PTX-nanocomplexes for uptake assays. For fluorescence microscopy and flow cytometry analysis, a red fluorescence (rhodamine 6G) labeled RVG-PTX-nanocomplex containing same amount of dye was treated to the cultures. The initial fluorescence levels of these three nanocomplexes stock suspension were compared and adjusted using IVIS Lumina System (Xenogen Corp., Alameda, CA) to make sure equal amount of initial fluorescence were used. At 1, 2 and 4 h, the cultures were washed three times with PBS. Fluorescence signals were first captured by fluorescence microscopy and then evaluated by flow cytometry. The intracellular fluorescence density indicated the uptake of RVG-PTX-nanocomplexes by BMM and neurons. To detect uptake of PTX content, BMM were treated with three sizes of RVG-PTX-nanocomplexes containing same concentration of PTX at 0.01 mg/mL. At the experimental time points, the supernatant and the cells were collected and PTX was extracted for HPLC assay. The PTX levels were calculated based on the positive control.

BMM release

For BMM release experiments, BMM cells were incubated with medium containing drug loaded nanocompexes at a concentration of 0.01 mg/mL (calculated as paclitaxel) for 4 h, then change with fresh medium. At fixed time points, the supernatant was change with fresh medium and collected for paclitaxel content assay. The samples were freeze-dried, thoroughly extracted with acetonitrile and the content of paclitaxel was examined by HPLC.

Statistical analyses

One-way analysis of variance was used to compare the treatment groups for each of the outcomes. Residual plots were examined to check whether the model assumptions were met. If the model assumptions were not met, then the $\log_{10}$ or square root transformation was applied to help with model fit. If the overall F-test was statistically significant, then pairwise comparisons were conducted, with adjustments made for multiple comparisons, using Tukey's method. *P* values less than 0.05 were considered to be statistically significant.

Results

Preparation of three sizes of RVG-PTX-nanocomplex

PTX-nanocomplex was formed as PLGA core and lipid shell structure. PTX loaded core was made by the nanoprecipitation [55,60-63] of PLGA, which is a non-cytotoxic and biodegradable polymer approved by FDA. The main content of HSPC is 1,2-dioctadecanoyl-sn-glycero-3-phosphoethanolcholine (DSPC), a phospholipid with an appropriate hydrophilic-lipophilic balance. HSPC was chosen as an emulsifier and turned into the monolayer surrounding the hydrophobic PLGA core. More importantly, DSPE-PEG-Mal, a PEGylated DSPE, was selected as an additive to the emulsifier which will intersperse in the phospholipid monolayer to form a PEG shell. The PEG long chain of DSPE-PEG-Mal provides electrostatic and steric stabilizations, a longer circulation half-life in vivo. In this study, the terminal maleimide group of the DSPE-PEG-Mal enables us to mount RVG, the targeting peptide, on the surface of nanocomplex. PTX loaded and fluorescence labeled nanocomplexes were obtained by mixing PTX and Rhodamine 6G with PLGA solution in the nanoprecipitation process.

By adjusting the PLGA polymer concentration we successfully obtained nanocomplexes with three typical sizes. The average size and size distribution of nanocomplexes were determined by Dynamic Light Scattering (DLS) measurement. The size of small-, medium- and large-size nanocomplexes were made as 220 ± 1.5, 137 ± 1.4 and 72 ± 2.7 nm with PDI 0.132, 0.165 and 0.189. PTX was successfully encapsulated in the hydrophilic inner core of the nanocomplex. As shown in Table 1, the drug-loading capacities of PTX were 2.7%, 1.4% and 1.1%, respectively. The corresponding encapsulation efficiencies were 27%, 14% and 11%, when the mass feed ratio of PTX and PLGA was fixed at 1 to 10.

RVG-PTX-nanocomplex was obtained by modifying PTX-nanocomplex with RVG [22-26] employing the specific bioconjugation reaction between thiol group of synthetic RVG peptide with cysteine C-terminal and Maleimide group of DSPE-PEG-Mal. The remaining maleimide groups on the surface of the nanocomplex provide the opportunity for further modification.

Characterization

There were increases of particle diameter and decreases of Zeta potential after PTX-nanocomplex conjugated with RVG (Table 1). These changes indicated the successful modification of PTX-nanocomplex by RVG peptide. The size distribution of RVG-PTX-nanocomplex was determined by DLS measurement Figure 1A. Visualization of the morphology by AFM showed that all three sizes of RVG-PTX-nanocomplexes had smooth and spheroid shape without aggregation Figure 1B. DLS measurement was used to characterize the small, medium and large sizes of PTX-nanocomplex with or without RVG modification, and the results are shown in Table 1.

The effect of size on PTX release from nanocomplex

The stability of RVG-PTX-nanocomplex was examined by analyzing PTX released from nanocarrier in phosphate buffered saline (PBS) at room temperature. Tween 80 was added into PBS to improve the solubility of PTX. The released PTX was separately collected from

	PLGA (mg/mL)	Lipid/ PLGA	Size (nm)	PTX loading (%)	Zeta potential	Encapsulation efficiency (%)
PTX-NPs (S)	3	1.2	72 ± 2.7	2.72 ± 0.09	-53 ± 1.3	27.2 ± 0.9
RVG-PTX-NPs (S)	3	1.2	73 ± 2.1	2.68 ± 0.12	-49 ± 0.9	26.8 ± 1.2
PTX-NPs (M)	8	0.8	137 ± 1.4	1.41 ± 0.15	-50 ± 1.7	14.1 ± 1.5
RVG-PTX-NPs (M)	8	0.8	139 ± 1.3	1.40 ± 0.13	-47 ± 1.4	14.0 ± 1.3
PTX-NPs (L)	50	0.6	220 ± 1.5	1.10 ± 0.06	-48 ± 1.6	11.0 ± 0.6
RVG-PTX-NPs (L)	50	0.6	222 ± 1.1	1.10 ± 0.11	-43 ± 2.1	11.0 ± 1.1

Data represent mean ± SE, n = 3.

Table 1: Characterization of three sizes of PTX-NPs and RVG-PTX-NPs.

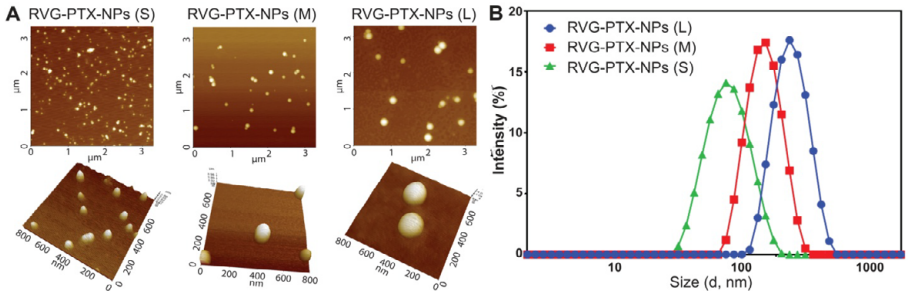

Figure 1: Characteriazation.

(A) Size and size distribution of RVG- PTX-nanocomplex by DLS analysis

(B) AFM images of RVG- PTX-nanocomplex

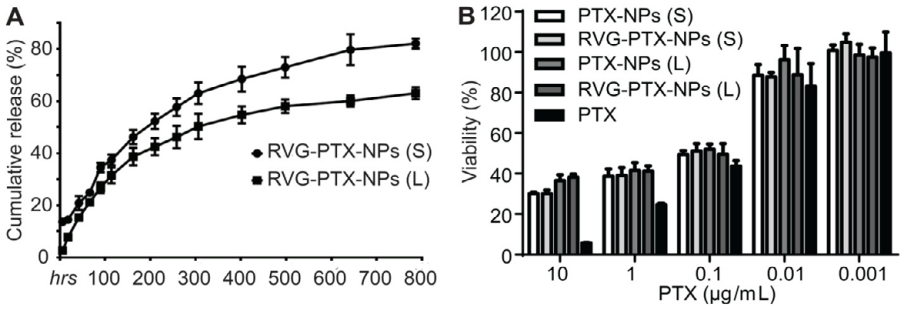

Figure 2: Stability and cytotoxicity.

The release of PTX from RVG-PTX-nanocomplexes was examined by HPLC

(A)In contrast to small-size RVG-PTX-nanocomplex (Nanocomplex-S), the larger one (Nanocomlex-L) showed slower controlled release over 786 h, indicating its greater stability. With 72 h treatment at various concentrations, dose dependent cytotoxicity of RVG-PTX-nanocomplex to U87 was detected by MTT assay

(B) The size changes and PTX-nanocomplex with or without RVG conjugation did not significantly influenced the cytotoxicity. RVG-PTX-nanocomplex displayed superior efficacy at 0.1 μg/ml

RVG-PTX-nanocomplexes by filtration process and quantitated by HPLC. The very slow release behaviors revealed the greater stability of RVG-PTX-nanocomplex Figure 2A. The small-size RVG-PTX-nanocomplex Figure 2, Nanocomplex-S showed a burst release of PTX at the first 6 h, and the cumulative release of PTX achieved 82% at 786 h. In contrast, large-size RVG-PTX-nanocomplex Figure 2, Nanocomplex-L did not exhibit a burst release and the cumulative release of PTX reached 63% at 786 hours. The release of PTX from large-size RVG-PTX-nanocomplex was relatively slower than that from the smaller one. We deduced that the slower degradation of large-size RVG-PTX-nanocomplex provided a very stable nanoformulation. The generally more sustained and controlled release profile of large-size RVG-PTX-nanocomplex facilitated the application for the delivery of anticancer drugs.

The effect of size on cytotoxicity

Human glioma U87 cells were treated with small-size and large-size RVG-PTX-nanocomplex and PTX-nanocomplex at varying concentrations (10^{-2}-10^{-5} mg/ml). We compared the large and the small particles to obtain more significant differences from the data. Free PTX served as a comparison to evaluate the glioma-specific cytotoxicity. Dose dependent cytotoxicity was seen in all groups. The therapeutic efficacy of small-size and large-size RVG-PTX-nanocomplex and PTX-nanocomplex were tested by measuring the U87 cells viability after 72 h Figure 2B. PTX packaged by nanocomplex displayed lower cytotoxicity to U87 cells than free PTX. No significant differences were obtained between the small- and the large-size RVG-PTX-nanocomplex and PTX-nanocomplex. The half maximal inhibitory concentration (IC50) of RVG-PTX-nanocomplex appeared at 10^{-4} mg/ml. RVG-PTX-nanocomplex displayed superior efficacy at 0.1 μg/ml. PTX loaded within nanocomplex indicated the effective anti-glioma activity. Our results indicated that the size modification of RVG-PTX-nanocomplex did not significantly affect cytotoxicity to U87. Because of PTX packaged within nanocomplex, the controlled release feature showed less toxicity than free PTX under the same concentration.

The effect of size on BMM and neurons uptake

To compare the size effect on uptake of small-, medium- and large-size RVG-PTX-nanocomplex by BMM and neurons, intracellular levels of fluorescence signal were evaluated after 1, 2 and 4 h incubation. We tested whether large-size RVG-PTX-nanocomplex facilitated BMM uptake, but stopped the neuronal uptake. Rhodamine 6G, a red fluorescent, was used to label RVG-PTX-NP and PTX-nanocomplex (data not shown). The amount of bound fluorescence was examined by

a live fluorescence imager system. BMM and the hippocampal neurons were treated three different sizes of RVG-PTX-nanocomplex, small-size Figure 3, Nanocomplex-S, medium-size Figure 3, Nanocomplex-M and large-size Figure 3, Nanocomplex-L containing the same amount of fluorescence. Fluorescence microscopy and flow cytometry assays were used to examine the level and quickness of uptake by BMM and neurons at 1, 2 and 4 h post-treatment.

The size increases in RVG-PTX-nanocomplex facilitated BMM uptake by fluorescence microscopy and flow cytometry assays Figure 3A and 3C. Comparable uptake of three different sizes of PTX-nanocomplexes showed that phagocytosis of BMM did not disturb by the physical property. Limited uptake of small-size RVG-PTX-nanocomplex by neurons was obtained at 4 h by fluorescence microscopy Figure 3B. Importantly, increase size of RVG-PTX-nanocomplex prevented uptake by neurons Figure 3B and 3D.

Quantitation of fluorescence intensity by flow cytometry assay was used to analyze the levels of RVG-PTX-nanocomplex taken by BMM and neurons Figure 3E. Results indicated that large-size RVG-PTX-nanocomplex provided the highest uptake levels in BMM. Increase the size of RVG-PTX-nanocomplex correlated to the enhanced uptake by BMM Figure 3E, upper panel. In contrast, increase of particle size prevented uptake of RVG-PTX-nanocomplex by neurons Figure

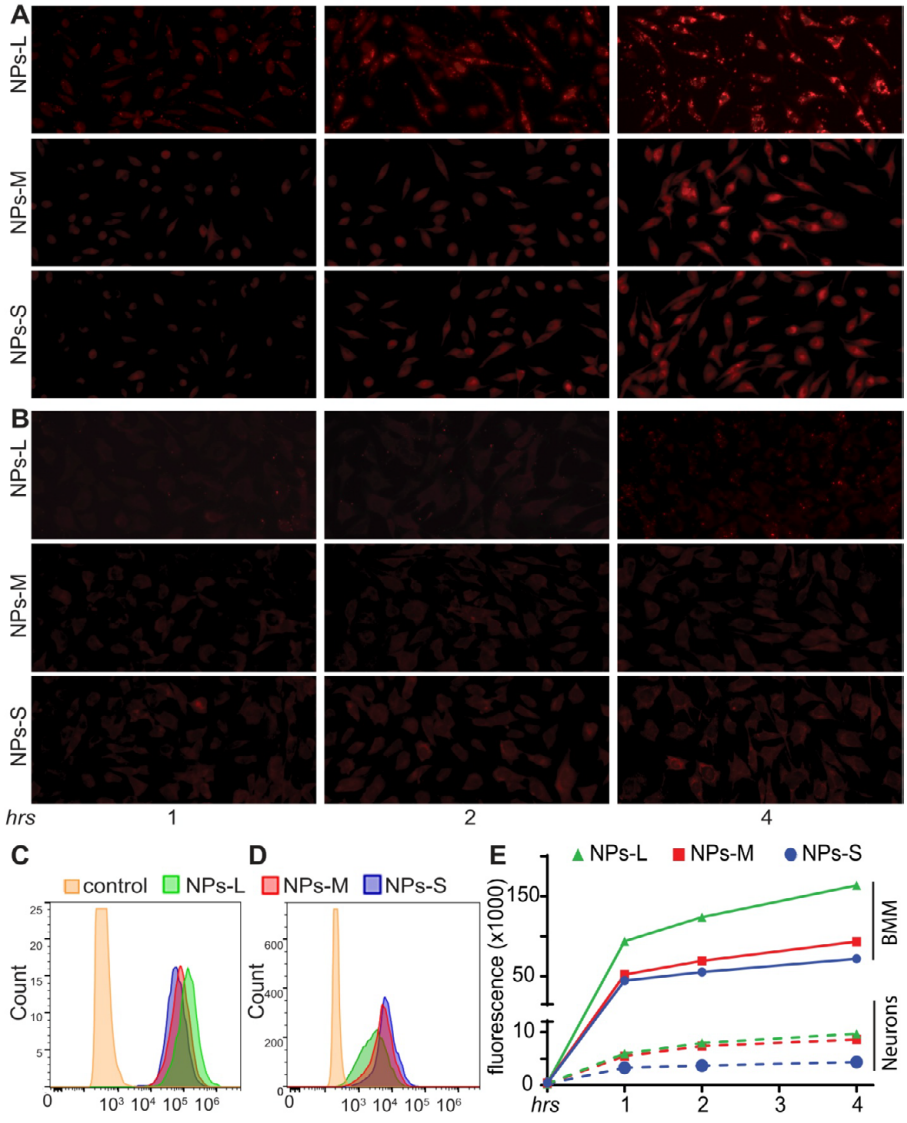

Figure 3: Uptake of RVG-PTX-nanocomplex by BMM and Neurons.

Small-, medium-, and large-sizes RVG-PTX-nanocomplex Nanocomplex-S, -M and -L were treated to BMM (A) and neurons (B) for 1, 2 and 4 hrs. Red fluorescence represented intracellular distribution of RVG-PTX-nanocomplex uptake by the cultures. Representative images of flow cytometry results exhibited the fluorescence signals in BMM (C) and neurons (D) at 4 hrs treated to three sizes of RVG-PTX-nanocomplexes. The shift of fluorescence distributions indicated the significant levels of all three sizes of RVG-PTX-nanocomplex uptake by BMM. Quantitation of flow cytometer assay (E) showed that large-size RVG-PTX-nanocomplex enhanced uptake by BMM. An increase uptake profile correlated to the rise of particle size. In contrast, enlarging size prevented neuronal uptake of RVG-PTX-nanocomplex. A decrease of uptake profile correlated to the rise of particle size.

3E, lower panel. The results confirmed that the biological functions of macrophages facilitated rapid uptake of large-size RVG-PTX-nanocomplex. Importantly, Increase the particle size stopped neurons to take RVG-PTX-nanocomplex.

Quantitation of intracellular PTX in BMM

To validate the transportation ability of three different sizes of RVG-PTX-nanocomplex, we examined uptake of PTX inside the BMM at 1, 2, 4 and 8 h. The intracellular PTX were extracted from fully washed BMM. RVG-PTX-nanocomplexes remaining in the medium were collected and PTX was extracted. HPLC assay was used to analyze PTX in BMM and medium. The levels of PTX were calculated as the percentage of initial incubating concentration. With the increase of incubation time, the amounts of PTX remaining within the medium were gradually decreased Figure 4A, upper panel. In contrast, intracellular PTX was increased in medium-size and large-size RVG-PTX-nanocomplexes treated BMM. Large-size RVG-PTX provided greater PTX levels with 25% of PTX within BMM at 8 h Figure 4B, lower panel. Small-size RVG-PTX-nanocomplexes treated BMM maintained a significant lower level of PTX at all the time points. This result was not in accordance with the result from microscopy and flow cytometry. We deduced that the smaller RVG-PTX-nanocomplexes were digested quickly after internalized by BMM cells and most of the released PTX inside the BMM cells binding to tubulin was hardly extracted by organic solvent. Large-size RVG-PTX-nanocomplex remained at stable formulation after internalized by BMM, leading to PTX easily extracted from cell lysate.

The effect of size on BMM release of RVG-PTX-nanocomplex

Major differences in the BMM release were achieved from different sizes of RVG-PTX-nanocomplex. The results were calculated as a percentage of PTX released to the medium Figure 4C. BMM release of PTX was up to several days. For the large-size RVG-PTX-nanocomplex, a robust release process was shown during the first 24 hours, and about 42% of the PTX was released to the medium from BMM by 5 days. Medium-size RVG-PTX-nanocomplex exhibited steady increases of released PTX in the medium, and reached 38% at day 5. Small-size RVG-PTX-nanocomplex revealed the lowest release profiles, and less than 9% of PTX was released from BMM into the medium at day 5. Thus, large-size RVG-PTX-nanocomplex released higher levels of PTX to the extracellular space. Because the side effects of PTX binding to tubulin had impact on BMM, MTT assay was used to examine cell viability after internalizing three sizes of RVG-PTX-nanocomplexes. Large-size RVG-PTX-nanocomplex loaded BMM showed greater viability than the small-size RVG-PTX-nanocomplex Figure 4D.

Correlation of RVG-AchR binding with TAM uptake

RVG peptide can specifically bind with the AchR and play a key role by crossing the BBB and entering the brain TAMs. Culture inserts were used to separately co-culture BMM and U87 to differentiate to tumor associated macrophages (TAMs). We made red fluorescence labeled HS-RVG directly reacted with TRM (HS - RVG + TRM), HS-RVG reduced by βME before reaction with TRM (HS – RVG + βME + TRM), and βME reaction with TRM without HS-RVG (βME + TRM). Macrophages were treated to HS – RVG + TRM, HS – RVG + βME + TRM and βME + TRM for 2 h. The specific binding only showed in

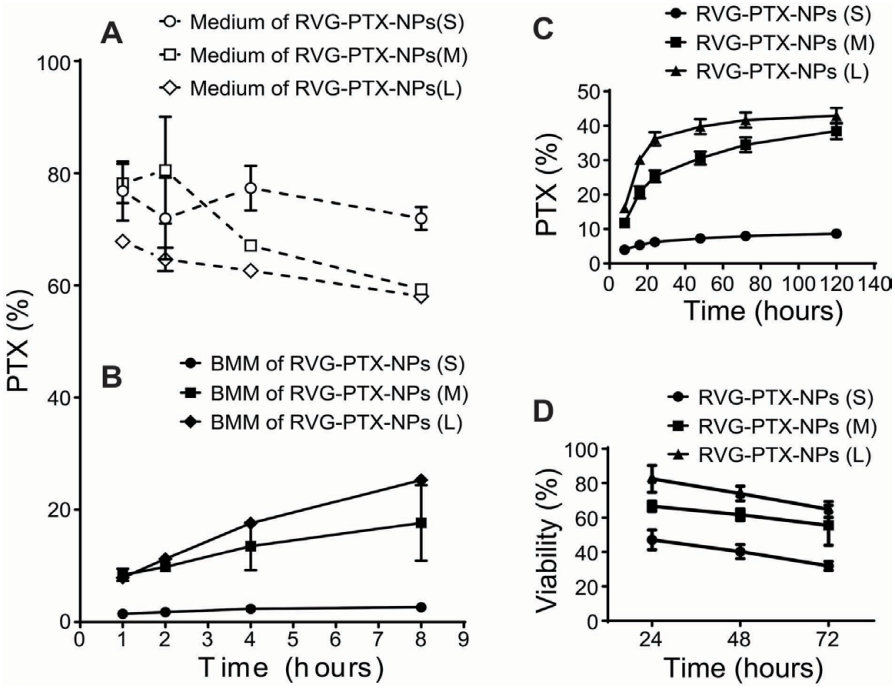

Figure 4: Quantitation of BMM uptake and release.
(A) Quantitative analysis of the PTX content inside the BMM cells
(B) and the PTX remained in the medium (A) after different co-incubation time
(C) The percentage of PTX content released by BMM to the medium
(D) The viability of BMM cells during the release period

HS – RVG – βME - TRM treated group Figure 5A, red. No specific binding signals were seen in cultures treated with HS-RVG-TRM or βME + TRM. The results further verified receptor-mediated RVG specific binding.

To study AchR expression correlated with uptake of RVG-PTX-nanocomplexes, antibody to AchR 7 was used to stain TAMs. High levels of AchR displayed in TAMs Figure 5B, green. The intracellular distribution of RVG-PTX-nanocomplexes uptake by TAMs Figure 5B, red correlated with AchR7 expression Figure 5B, merge.

Transportation of RVG-PTX-nanocomplex from TAMs to U87

RVG-PTX-nanocomplex uptake by TAMs was transported to the neighboring U87 via cell-to-cell direct interaction. TAMs were pre-loaded with red fluorescence labeled RVG-PTX-nanocomplexes Figure 6, red, and then co-cultured with GFP-U87 Figure 6, green. In the mixed cultures, the red RVG-PTX-nanocomplexes loaded TAMs and the green U87 cells allowed visualizing the cell-to-cell transportation of RVG-PTX-Nanocomplex. The first 12 h, "nano-synaptic"-like contact Figure 6A, arrow were seen between the red RVG-PTX-NP loaded TAMs and green U87. Fluorescence images clearly showed the red RVG-PTX-nanocomplexes transporting from the TAMs cytoplasm into U87 Figure 6B. Enlarged image Figure 6C exhibited RVG – PTX - nanocomplexes transportation via TAM extended process Figure 6C, arrow.

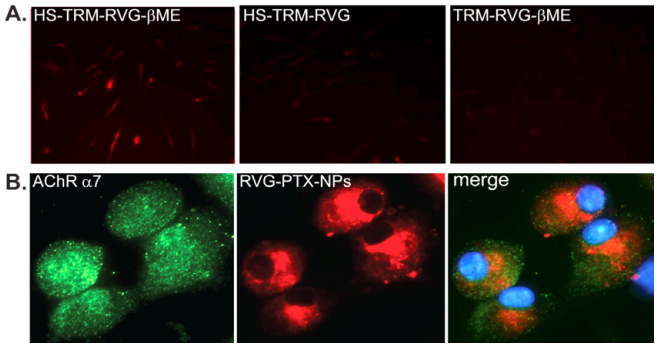

Figure 5: RVG mediated TAMs specificity.

The specific RVG binding shown in HS-RVG+βME+TRM treated cells at 2 hrs incubation (A, red signals). No specific binding signals seen in cultures treated with RVG without functional structure (HS-RVG-TRM) or no fluorescence labeling (bME-TRM). The untreated TAMs served as control. RVG binding to AchR mediated RVG-PTX-nanocomplex uptake was analyzed by immunostaining with antibody to AchR7 (B, green). High levels of AchR expressed in TAMs, which had taken up RVG-PTX-nanocomplex (B, red) to display a correlated intracellular distribution (B, merge).

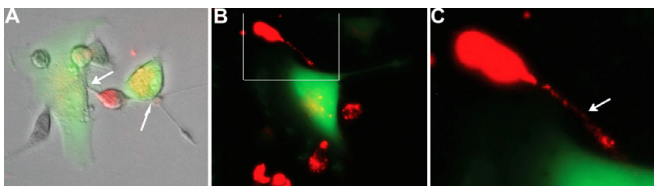

Figure 6: Pre-loaded TAMs transporting RVG-PTX-nanocomplexes to U87 cells.

RVG-PTX-nanocomplex pre-loaded TAMs (red, nano*-TAMs) were co-cultured with GFP-U87 (green). At first 12 h, fluorescence images showed that nano*-TAMs transported red RVG-PTX-nanocomplexes into U87 via cell-to-cell direct transportation (A, arrow). The red "nanocomplexes" co-localized with GFP resulted as yellow in U87 cell bodies (A and B). Enlarged image (C) showed the "red-nanocomplexes" transporting to green U87 by TAMs process connection.

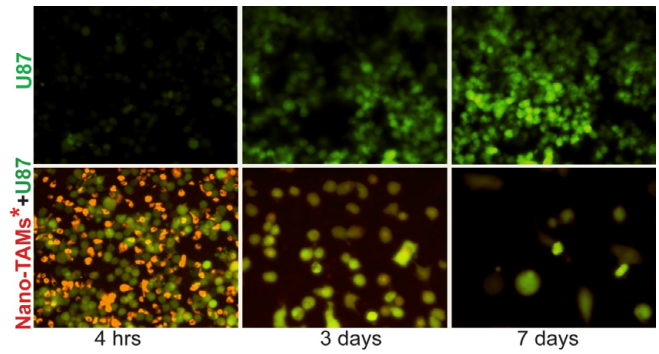

Figure 7: Anti-glimoa activities.

Microscopy was used to detect GFP-U87 cells (green) co-cultured with large-size RVG-PTX-nanocomplex loaded TAMs (Nano-TAMs, red). Anti-glioma activity of Nano-TAMs showed significant killing of U87 at 3 and 7 days when compared to U87 alone. No red Nano-TAMs were seen at day 7 due to release of red RVG-PTX-nanocomplex.

Anti-glioma activities of RVG-PTX-nanocomplex loaded TAMs

We further investigated whether RVG-PTX-nanocomplex engulfed by TAMs can actively kill glioma cells. RVG - PTX -nanocomplexes were pre-loaded to TAMs (Nano-TAMs). Nano-TAMs Figure 7, red were co-cultured with U87 cells Figure 7, green, at a ratio of 1:1, and continually cultured up to 7 days. U87 cell served as control Figure 7, upper panel. After 4 h of co-culture, red RVG-PTX-nanocomplexes transporting into U87 showed as "yellow" U87 cells Figure 7, lower panel. On co-cultivation days 3 and 7, fluorescence images showed significant killing of U87 cells compared to the controls. Dual fluorescence images showed that no red Nano-TAMs were detected at days 3 and 7 of co-cultivation, indicating RVG-PTX-nanocomplexes release and transportation to the U87 cells. The data further confirmed RVG-PTX-nanocomplex targeted to TAMs to actively deliver PTX to neighboring cancer cells, providing significant cytotoxicity.

Discussion

Nanoprecipitation is one of the most important methods for the preparation of nanocomplex. Compared with other methods, such as emulsion, it has the advantages of size modification [56-63]. When employing nanoprecipitation, the particle size can be rationally predicted by solvent type, polymer concentration, and solvent to water ratio. Particularly, there is a linear correlation between polymer concentrations and volumetric sizes of the resulting nanocomplex.

The physicochemical properties of nanocomplex play critical roles in cell uptake and pharmacokinetics. The core-shell nanocomplex was capable of loading PTX inside and conjugating targeting peptide RVG on the surface. Three sizes of RVG-PTX-nanocomplex increased to about twice their size. The smaller size of RVG-PTX Nanocomplex had higher PTX loading. The increases of size in RVG-PTX-nanocomplex prevented uptake by neurons. The size-dependent uptake, release and TAMs targeting specificity of RVG-PTX-nanocomplex were more prominent between the sizes of 73 nm and 222 nm. Large-size RVG-PTX-nanocomplex exhibited increases in uptake and release by BMM. The particle size of RVG-PTX-nanocomplex had significant effects

on TAMs targeting specificity and pharmacokinetics. In this study, we optimized the most influencing factor, particle size, to develop a brain-TAMs targeted delivery system. Three different sizes of RVG-conjugated core-shell structural nanoparticles were successfully prepared. By adjusting the PLGA polymer concentration, RVG-PTX-nanocomplex was successfully made with size of ~ 73 nm, ~ 139 nm, and ~ 222 nm. Since these particles had identical structure, chemical components and surface properties except for their different size, the small-, medium-, and large-size RVG-PTX-nanocomplex provide excellent models to study size-dependent biological behaviors.

The internalization of three sizes of nanoparticles by BMM was very similar. Among these three sizes of nanocomplex, the large-size RVG-PTX-nanocomplex has generally had a more sustained and controlled release profile *in vitro* due to the relatively slower degradation than the smaller ones. After uptake by BMM, free PTX was released faster from small-size RVG-PTX-nanocomplex leading to a greater cytotoxicity than large-size RVG-PTX-nanocomplex. The released PTX binds to tubulin preventing its transportation from BMM to extracellular medium. It is well known that the release behavior of PLGA nanoparticles can be regulated by the ratio of the composition of LA units and GA units. Our results demonstrated that the increase of particle size, by changing the PLGA polymer concentration, prolonged PTX release from nanocomplex. From this study, we found that the difference in size of RVG-PTX-nanocomplex did not affect cytotoxicity to tumor cells. Although slower release of large-RVG-PTX-nanocomplex had less initial toxic to tumor cells, the prolonged and consistent PTX was transported to the cancer cell, leading to potential improved pharmacokinetic and enhanced therapeutic efficacy in clinical use.

The cell-to-cell transportation revealed initial localized distribution of RVG-PTX-nanocomplex in the targeted TAMs at the sites of glioma contact with the neighboring tumor cells. Cell-to-cell contact plays an important role in the "nano-synaptic"-like transportation. Thus, co-culture of pre-loaded macrophages with U87, transferred a significant amount of RVG-PTX-nanocomplex to produce greater antiglioma activities. In particular, pre-loaded TAMs delivered a greater amount of RVG-PTX-nanocomplex into intracellular of U87 cells. It is likely that "nano-synaptic"-like transportation is involved in this TAMs mediated delivery system.

The design of a single cell-based delivery system, targeting efficiency and specificity with minimal off-target effects, remains to be a major challenge. The advantage of this delivery system is that it combined a high expression of AChR and strong phagocytosis of TAMs, providing the selective targeting specificity. The ability of macrophages to uptake RVG-PTX-nanocomplex, release drugs and accumulate within the brain tumors makes them attractive targets for glioma therapy. Although changing the size of RVG-PTX-nanocomplex greatly influenced the neurons uptake behavior, the strong phagocytosis of macrophages exhibited greater uptake of RVG-PTX-nanocomplex without rejection by increasing the particle size. Most importantly, RVG-PTX-nanocomplex uptake by neurons was particularly limited by the particle size. We developed the size-controlled RVG-PTX-nanocomplex for selective uptake by TAMs with off-neurons effect. With selective TAMs uptake and effective PTX transportation and U87 cytotoxicity, large-size RVG-PTX-nanocomplex offer greater therapeutic potential for anti-glioma therapy. On the other hand, small-size RVG-PTX nanocomplex are more easily internalized by normal cells, leading to off-target side effects.

Conclusions

In this study, we developed three sizes of PTX loaded nanocomplex mounted with RVG peptide. The size-controlled RVG-PTX-nanocomplex for TAMs targeted delivery to treat glioma was investigated. We found that large-size RVG-PTX-nanocomplex had better controlled release, selective TAMs uptake and effective U87 cytotoxicity with off-neurons effect. We concluded that our "larger" RVG-PTX-nanocomplex (139-222 nm) can have a more promising potential when used in TAMs targeted delivery system for the treatment of glioma.

Acknowledgements

We gratefully thank Adrienne Nevarez, Sylvia Rodriguez, Leslie Casas, and Gloria Chavez for critical reading of this manuscript and outstanding administrative support. Texas Tech University Health Sciences Center Start-Up Fund and TTUHSC Seed grant supported this work.

References

1. Giese A, Westphal M (1996) Glioma invasion in the central nervous system. Neurosurgery 39: 235-250.
2. Furnari FB, Fenton T, Bachoo RM, Mukasa A, Stommel JM, et al. (2007) Malignant astrocytic glioma: genetics, biology, and paths to treatment. Genes Dev 21: 2683-2710.
3. Wiesner SM, Freese A, Ohlfest JR (2005) Emerging concepts in glioma biology: implications for clinical protocols and rational treatment strategies. Neurosurg Focus 19: E3.
4. Preusser M, Haberler C, Hainfellner JA (2006) Malignant glioma: neuropathology and neurobiology. Wien Med Wochenschr 156: 332-337.
5. Pazdur R, Kudelka AP, Kavanagh JJ, Cohen PR, Raber MN (1993) The taxoids: paclitaxel (Taxol) and docetaxel (Taxotere). Cancer Treat Rev 19: 351-386.
6. Tao Y, Han J, Dou H (2012) Surface modification of paclitaxel-loaded polymeric nanoparticles: Evaluation of in vitro cellular behavior and in vivo pharmacokinetic. Polymer 53: 5078-5086.
7. Zhang JA, Anyarambhatla G, Ma L, Ugwu S, Xuan T, et al. (2005) Development and characterization of a novel Cremophor EL free liposome-based paclitaxel (LEP-ETU) formulation. Eur J Pharm Biopharm 59: 177-187.
8. Yang T, Cui FD, Choi MK, Lin H, Chung SJ, et al. (2007) Liposome formulation of paclitaxel with enhanced solubility and stability. Drug Deliv 14: 301-308.
9. Elkharraz K, Faisant N, Guse C, Siepmann F, Arica-Yegin B, et al. (2006) Paclitaxel-loaded microparticles and implants for the treatment of brain cancer: preparation and physicochemical characterization. Int J Pharm 314: 127-136.
10. Tao Y, Han J, Wang X, Dou H (2013) Nano-formulation of paclitaxel by vitamin E succinate functionalized pluronic micelles for enhanced encapsulation, stability and cytotoxicity. Colloids Surf B Biointerfaces 102: 604-610.
11. Tao Y, Ning M, Dou H (2013) A novel therapeutic system for malignant glioma: nanoformulation, pharmacokinetic, and anticancer properties of cell-nano-drug delivery. Nanomedicine: Nanotechnology, Biology and Medicine 9: 222-232.
12. Tao YH, Han JF, Dou HY (2012) Brain-targeting gene delivery using a rabies virus glycoprotein peptide modulated hollow liposome: bio-behavioral study. Journal of Materials Chemistry 22: 11808-11815.
13. Tao YH, Han JF, Dou HY, Ye C, Thomas T, (2012) Reduction-responsive gold-nanoparticle-conjugated Pluronic micelles: an effective anti-cancer drug delivery system. Journal of Materials Chemistry 22: 18864-18871.
14. Li C, Yu DF, Newman RA, Cabral F, Stephens LC, et al. (1998) Complete regression of well-established tumors using a novel water-soluble poly(L-glutamic acid)-paclitaxel conjugate. Cancer Res 58: 2404-2409.
15. Khandare JJ, Jayant S, Singh A, Chandna P, Wang Y, et al. (2006) Dendrimer versus linear conjugate: Influence of polymeric architecture on the delivery and anticancer effect of paclitaxel. Bioconjug Chem 17: 1464-1472.
16. Potineni A, Lynn DM, Langer R, Amiji MM (2003) Poly(ethylene oxide)-modified poly(beta-amino ester) nanoparticles as a pH-sensitive biodegradable system for paclitaxel delivery. Journal of Controlled Release 86: 223-234.

17. Wu J, Liu Q, Lee RJ (2006) A folate receptor-targeted liposomal formulation for paclitaxel. Int J Pharm 316: 148-153.

18. Chen X, Plasencia C, Hou Y, Neamati N (2005) Synthesis and biological evaluation of dimeric RGD peptide-paclitaxel conjugate as a model for integrin-targeted drug delivery. J Med Chem 48: 1098-1106.

19. Pan J, Feng SS (2008) Targeted delivery of paclitaxel using folate-decorated poly(lactide)-vitamin E TPGS nanoparticles. Biomaterials 29: 2663-2672.

20. Danhier F, Vroman B, Lecouturier N, Crokart N, Pourcelle V, et al. (2009) Targeting of tumor endothelium by RGD-grafted PLGA-nanoparticles loaded with paclitaxel. J Control Release 140: 166-173.

21. Bradley MO, Webb NL, Anthony FH, Devanesan P, Witman PA, et al. (2001) Tumor targeting by covalent conjugation of a natural fatty acid to paclitaxel. Clin Cancer Res 7: 3229-3238.

22. Kumar P, Wu H, McBride JL, Jung KE, Kim MH, et al. (2007) Transvascular delivery of small interfering RNA to the central nervous system. Nature 448: 39-43.

23. Hwang DW, Son S, Jang J, Youn H, Lee S, et al. (2011) A brain-targeted rabies virus glycoprotein-disulfide linked PEI nanocarrier for delivery of neurogenic microRNA. Biomaterials 32: 4968-4975.

24. Liu Y, Huang R, Han L, Ke W, Shao K, et al. (2009) Brain-targeting gene delivery and cellular internalization mechanisms for modified rabies virus glycoprotein RVG29 nanoparticles. Biomaterials 30: 4195-4202.

25. Gao Y, Wang T, Wang S, Jiang T (2013) RVG peptide tethered polyethyleneglycol-graft-trimethyl chitosan copolymers for transvascular delivery of siRNA to the brain. Journal of Controlled Release 172: e120.

26. Gao Y, Wang ZY, Zhang J, Zhang Y, Huo H, et al. (2014) RVG-peptide-linked trimethylated chitosan for delivery of siRNA to the brain. Biomacromolecules 15: 1010-1018.

27. Pulford B, Reim N, Bell A, Veatch J, Forster G, et al. (2010) Liposome-siRNA-Peptide Complexes Cross the Blood-Brain Barrier and Significantly Decrease PrP^{C} on Neuronal Cells and PrP^{RES} in Infected Cell Cultures. PLoS ONE 5: e11085.

28. Zhan C, Li B, Hu L, Wei X, Feng L, et al. (2011) Micelle-Based Brain-Targeted Drug Delivery Enabled by a Nicotine Acetylcholine Receptor Ligand. Angewandte Chemie International Edition 50: 5482-5485.

29. Alvarez-Erviti L, Seow Y, Yin H, Betts C, Lakhal S, et al. (2011) Delivery of siRNA to the mouse brain by systemic injection of targeted exosomes. Nat Biotechnol 29: 341-345.

30. Anzimirov VL, Romanova NV, Zhukov PV (1997) [The orthostatic resistance of the cerebral and peripheral circulations in patients with contusive brain lesions]. Zh Vopr Neirokhir Im N N Burdenko : 20-23.

31. Cenna J, Tan GS, Papaneri AB, Dietzschold B, Schnell MJ, et al. (2008) Immune modulating effect by a phosphoprotein-deleted rabies virus vaccine vector expressing two copies of the rabies virus glycoprotein gene. Vaccine 26: 6405-6414.

32. Son S, Hwang do W, Singha K, Jeong JH, Park TG, et al. (2011) RVG peptide tethered bioreducible polyethylenimine for gene delivery to brain. J Control Release 155: 18-25.

33. Xiang L, Zhou R, Fu A, Xu X, Huang Y, et al. (2011) Targeted delivery of large fusion protein into hippocampal neurons by systemic administration. J Drug Target 19: 632-636.

34. Hussain SF, Yang D, Suki D, Aldape K, Grimmet E, et al. (2006) The role of human glioma-infiltrating microglia/macrophages in mediating antitumor immune responses. Neuro Oncol 8: 261-279.

35. Deininger MH, Meyermann R, Schluesener HJ (2003) Expression and release of CD14 in astrocytic brain tumors. Acta Neuropathol 106: 271-277.

36. Kennedy BC, Maier LM, D'Amico R, Mandigo CE, Fontana EJ, et al. (2009) Dynamics of central and peripheral immunomodulation in a murine glioma model. BMC Immunol 10: 11.

37. Zhang L, Handel MV, Schartner JM, Hagar A, Allen G, et al. (2007) Regulation of IL-10 expression by upstream stimulating factor (USF-1) in glioma-associated microglia. J Neuroimmunol 184: 188-197.

38. Watters JJ, Schartner JM, Badie B (2005) Microglia function in brain tumors. J Neurosci Res 81: 447-455.

39. Morioka T, Baba T, Black KL, Streit WJ (1992) Immunophenotypic analysis of infiltrating leukocytes and microglia in an experimental rat glioma. Acta Neuropathol 83: 590-597.

40. Nagai T, Tanaka M, Tsuneyoshi Y, Xu B, Michie SA, et al. (2009) Targeting tumor-associated macrophages in an experimental glioma model with a recombinant immunotoxin to folate receptor beta. Cancer Immunol Immunother 58: 1577-1586.

41. Cole AJ, David AE, Wang J, Galbán CJ, Hill HL, et al. (2011) Polyethylene glycol modified, cross-linked starch-coated iron oxide nanoparticles for enhanced magnetic tumor targeting. Biomaterials 32: 2183-2193.

42. Chen H, Wang L, Yeh J, Wu X, Cao Z, et al. (2010) Reducing non-specific binding and uptake of nanoparticles and improving cell targeting with an antifouling PEO-b-PgammaMPS copolymer coating. Biomaterials 31: 5397-5407.

43. Chaudhuri RG, Paria S, (2012) Core/Shell Nanoparticles: Classes, Properties, Synthesis Mechanisms, Characterization, and Applications. Chemical Reviews 112: 2373-2433.

44. Malam Y, Loizidou M, Seifalian AM (2009) Liposomes and nanoparticles: nanosized vehicles for drug delivery in cancer. Trends in Pharmacological Sciences 30: 592-599.

45. Sharma A, Sharma US (1997) Liposomes in drug delivery: Progress and limitations. International Journal of Pharmaceutics 154: 123-140.

46. Jiang W, Kim BY, Rutka JT, Chan WC (2008) Nanoparticle-mediated cellular response is size-dependent. Nat Nanotechnol 3: 145-150.

47. Foged C, Brodin B, Frokjaer S, Sundblad A (2005) Particle size and surface charge affect particle uptake by human dendritic cells in an in vitro model. Int J Pharm 298: 315-322.

48. Zhang S, Li J, Lykotrafitis G, Bao G, Suresh S (2009) Size-Dependent Endocytosis of Nanoparticles. Advanced Material 21: 419-424.

49. Beduneau A, Ma Z, Grotepas CB, Kabanov A, Rabinow BE, et al. (2009) Facilitated monocyte-macrophage uptake and tissue distribution of superparmagnetic iron-oxide nanoparticles. PLoS One 4: e4343.

50. Dou H, Destache CJ, Morehead JR, Mosley RL, Boska MD, et al. (2006) Development of a macrophage-based nanoparticle platform for antiretroviral drug delivery. Blood 108: 2827-2835.

51. Dou H, Grotepas CB, McMillan JM, Destache CJ, Chaubal M, et al. (2009) Macrophage delivery of nanoformulated antiretroviral drug to the brain in a murine model of neuroAIDS. J Immunol 183: 661-669.

52. Nowacek AS, Miller RL, McMillan J, Kanmogne G, Kanmogne M, et al. (2009) NanoART synthesis, characterization, uptake, release and toxicology for human monocyte–macrophage drug delivery. Nanomedicine 4: 903-917.

53. Govender T, Stolnik S, Garnett MC, Illum L, Davis SS (1999) PLGA nanoparticles prepared by nanoprecipitation: drug loading and release studies of a water soluble drug. J Control Release 57: 171-185.

54. Tang L, Yang X, Yin Q, Cai K, Wang H, et al. (2014) Investigating the optimal size of anticancer nanomedicine. Proc Natl Acad Sci U S A 111: 15344-15349.

55. Dong Y, Feng SS (2004) Methoxy poly(ethylene glycol)-poly(lactide) (MPEG-PLA) nanoparticles for controlled delivery of anticancer drugs. Biomaterials 25: 2843-2849.

56. Chan JM, Zhang L, Tong R, Ghosh D, Gao W, et al. (2010) Spatiotemporal controlled delivery of nanoparticles to injured vasculature. Proc Natl Acad Sci U S A 107: 2213-2218.

57. Chan JM, Zhang L, Yuet KP, Liao G, Rhee JW, et al. (2009) PLGA-lecithin-PEG core-shell nanoparticles for controlled drug delivery. Biomaterials 30: 1627-1634.

58. Zhang L, Chan JM, Gu FX, Rhee JW, Wang AZ, et al. (2008) Self-assembled lipid--polymer hybrid nanoparticles: a robust drug delivery platform. ACS Nano 2: 1696-1702.

59. Aubry J, Ganachaud F, Cohen Addad JP, Cabane B (2009) Nanoprecipitation of polymethylmethacrylate by solvent shifting: 1. Boundaries. Langmuir 25: 1970-1979.

60. Fessi H, Puisieux F, Devissaguet J Ph, Ammoury N, Benita S (1989) Nanocapsule formation by interfacial polymer deposition following solvent displacement. International Journal of Pharmaceutics 55: R1-R4.

61. Horni S, Heinzeet T, Becer CR, Schubert US (2009) Synthetic polymeric nanoparticles by nanoprecipitation. Journal of Materials Chemistry 19: 3838-3840.

62. Schubert S, Delaney JJT, Schubert US (2011) Nanoprecipitation and nanoformulation of polymers: from history to powerful possibilities beyond poly (lactic acid). Soft Matter 7: 1581-1588.

63. Cheng J, Teply BA, Sherifi I, Sung J, Luther G, et al. (2007) Formulation of functionalized PLGA-PEG nanoparticles for in vivo targeted drug delivery. Biomaterials 28: 869-876.